Redox-Active Tyrosine Residues in Pentapeptides

Ilya R. Vassiliev,† Adam R. Offenbacher, and Bridgette A. Barry*

School of Chemistry and Biochemistry and Parker H. Petit Institute for Bioengineering and Bioscience, Georgia Institute of Technology, Atlanta, Georgia 30332-0363

Received: July 27, 2005; In Final Form: September 21, 2005

Tyrosyl radicals are important in long-range electron transfer in several enzymes, but the protein environmental factors that control midpoint potential and electron-transfer rate are not well understood. To develop a more detailed understanding of the effect of protein sequence on their photophysical properties, we have studied the spectroscopic properties of tyrosyl radicals at 85 K. Tyrosyl radical was generated by UV-photolysis of pentapeptides in polycrystalline samples. The sequence of the pentapeptides was chosen to mimic peptide sequences found in redox-active tyrosine containing enzymes, ribonucleotide reductase and photosystem II. From EPR studies, we report that the EPR line shape of the tyrosyl radical depends on peptide sequence. We also present the first evidence for a component of the tyrosyl radical EPR signal, which decays on the seconds time scale at 85 K. We suggest that this transient results from a spontaneous, small conformational rearrangement in the radical. From FT-IR studies, we show that amide I vibrational bands (1680−1620 cm^{-1}) and peptide bond skeletal vibrations (1230−1090 cm^{-1}) are observed in the photolysis spectra of tyrosine-containing pentapeptides. From these data, we conclude that oxidation of the tyrosine aromatic ring perturbs the electronic structure of the peptide bond in tyrosine-containing oligopeptides. We also report sequence-dependent alterations in these bands. These results support the previous suggestion (*J. Am. Chem. Soc.* **2002**, *124,* 5496) that spin delocalization can occur from the tyrosine aromatic ring into the peptide bond. We hypothesize that these sequence-dependent effects are mediated either by electrostatics or by changes in conformer preference in the peptides. Our findings suggest that primary structure influences the functional properties of redox-active tyrosines in enzymes.

The aromatic side chain of tyrosine can participate in long-distance electron-transfer reactions in enzymes. In many cases, these electron-transfer reactions are essential steps in the enzyme's catalytic mechanism. For example, one-electron oxidation/reduction of a tyrosine side chain occurs in prostaglandin H synthase,[1] galactose oxidase,[2] ribonucleotide reductase (RNR)[3] and photosystem II (PS II).[4,5] While there have been previous model compound studies of tyrosyl and phenoxyl radical structure (see, for example, refs 6−13), the influence of peptide bond formation on the structure, function, and redox potential of the radical is not well understood.

EPR (electron paramagnetic resonance) studies have shown that the unpaired electron spin of the tyrosyl radical is primarily located on the aromatic ring, with maximum densities at the 1′, 3′ and 5′ positions.[11−15] Similar spin density distributions have been reported for the $Y122^{\bullet}$ and $Y160^{\bullet}$ radicals in RNR and PSII.[3,12,16−18]

However, it is clear that the protein environment of the tyrosine can control the function of the redox active amino acid.[19,20] One mechanism of redox potential control is suggested by recent DFT (density functional theory) calculations on tyrosyl radical, which report that spin density delocalizes to the terminal groups of tyrosine.[13] Of particular interest is the fact that the amount of spin density delocalization was predicted to be conformation-dependent. This conformation dependence offers a method for midpoint potential control,[20,21] because there is a correlation between increased spin delocalization and decreases in midpoint potential (reviewed in ref 22). In previous DFT calculations, the amount of spin density on the amino nitrogen of tyrosyl radical was predicted to be 0.016 in the Boltzmann averaged conformation.[13] The predicted ^{14}N hyperfine interaction is less than ∼0.4 G for X-band EPR. Thus, this amount of spin density delocalization is small and would not be detected by field-swept EPR techniques alone.[13] Interestingly, a coupling, which was attributed to the amide nitrogen, was detected in previous ESEEM studies of a PSII tyrosyl radical.[23] A possible, small amount of spin density delocalization in tyrosyl radical is thus easily reconcilable with previous conclusions that the sum of the spin density on the aromatic ring and the oxygen is close to one.[11,12,14]

While this predicted amount of spin density delocalization to terminal groups is small, it may be significant, particularly if it is sensitive to conformation or electrostatics. The significance could arise from control of midpoint potential, as discussed above, or from a directional control mechanism.[20] Because it is difficult to detect a small hyperfine splitting with field swept EPR spectroscopy, we used Fourier transform infrared (FT-IR) spectroscopy to test this theoretical prediction.[13] In this technique, UV photolysis pulses are applied to produce a tyrosyl radical, and FT-IR spectra are collected before and after illumination and are subtracted to construct a photolysis-induced difference spectrum. This spectrum is exquisitely sensitive to small changes in force constant. DFT calculations predicted that spin density delocalization would upshift the frequency of the amino NH bending mode.[13,24] Such an upshift was indeed detected in the photolysis FT-IR spectrum of tyrosyl radical, and the vibrational band was shown to be ^{15}N sensitive,

* To whom correspondence should be addressed. E-mail: bridgette.barry@chemistry.gatech.edu.

† Deceased August 10, 2005.

10.1021/jp054159f CCC: $30.25
Published on Web 11/12/2005

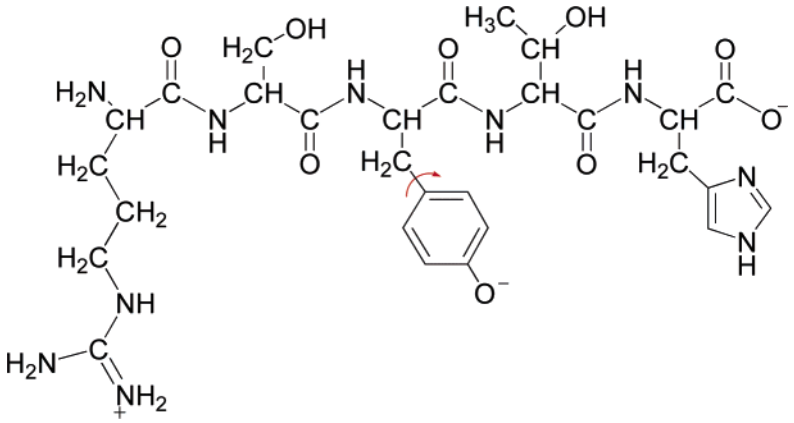

Figure 1. Structure of pentapeptide RSYTH, which is the sequence surrounding the tyrosyl radical in the R2 subunit of *Escherichia coli* RNR. The arrow shows the rotation of the aromatic ring along the $C_{1'}$-C_{β} bond.

as expected.[13] In addition, when tyrosyl radical was generated by photolysis in some tyrosine-containing dipeptides, a contribution to the FT-IR spectrum from the amide I and II (peptide bond) vibrational bands was observed.[13] Taken together, these results suggest that spin density delocalization occurs in tyrosinate and tyrosine-containing dipeptides.

The question addressed in this paper is whether spin density delocalization can occur when tyrosyl radicals are formed in oligopeptides and, if so, whether this effect is sensitive to sequence.[13,25] Accordingly, we report the results of EPR and FT-IR studies of tyrosyl radicals generated in pentapeptides. The primary sequences of the pentapeptides used in our study were based on sequences containing redox-active tyrosine residues in two enzymes—PS II and RNR (Figure 1).[26,27]

Materials and Methods

Samples. L-Tyrosine (denoted as Y in the figures), boric acid, sodium hydroxide, and hydrochloric acid were purchased from Sigma (St. Louis, MO). Polyalanine (MW 1000−5000) was purchased from MP Biomedicals, LLC (Aurora, OH). The tyrosine-containing dipeptide IY and a control dipeptide, RE, were purchased from Bachem (King of Prussia, PA). The tyrosine-containing pentapeptides, IYPIG, EYPIG, RYPIG, and RSYTH were purchased from Sigma-Genosys (The Woodlands, TX). The pentapeptide samples were purified by the manufacturer on Discovery Bio Wide Pore C-18 column (mobile phase A, 0.1% TFA/water; mobile phase B, 0.1% TFA/acetonitrile). The purity of each sample was assessed from the chromatograms, monitored at 214 nm, and was reported in the range from 94 to 99% homogeneity. The UV−visible absorption spectra of the samples were recorded at 100 μM concentration in 1 cm quartz cuvettes on a Hitachi U-3000 spectrophotometer (Figure 2). As shown in Figure 2, the spectra of pentapeptides, tyrosinate, and the dipeptide, IY, were similar. The extinction coefficients of these compounds at 266 nm (used as the excitation wavelength for generation of tyrosyl radicals) were also similar, with values between 890 and 1000 M^{-1} cm^{-1}.

The sequences of pentapeptides were chosen to maximize the solubility of the synthesized peptides. The pentapeptide, IYPIG, represents the sequence containing the redox-active tyrosine, Y160, in a cyanobacterial PSII D1 subunit (NCBI entry, NP_682634[26]). Two other pentapeptides, EYPIG and RYPIG, are variants of the D1 sequence, in which the amino terminal isoleucine has been replaced by a glutamic acid or an arginine. This change in primary sequence should have the effect of modulating peptide charge. The *Protparam*-predicted isoelectric points are 4.0 for EYPIG, 5.5 for IYPIG, and 8.8 for

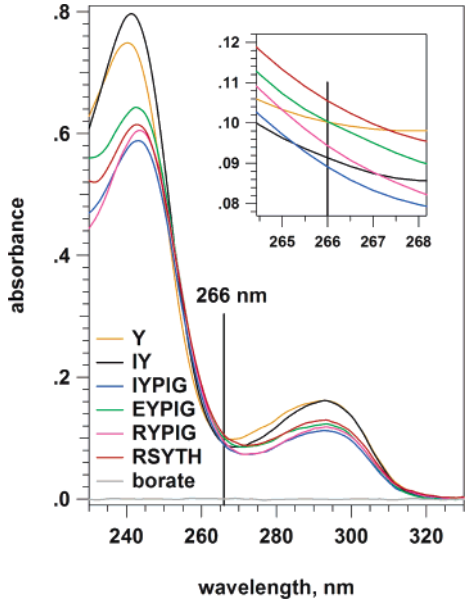

Figure 2. Room temperatureabsorption spectra of tyrosinate, dipeptide IY, pentapeptides (relative to borate buffer) and borate buffer (relative to water) measured at 1 cm path length. The inset shows the spectral absorption at 266 nm wavelength, which is the wavelength used for photolysis.

RYPIG (http://us.expasy.org/tools/protparam.html). The pentapeptide, RSYTH, shown in Figure 1, is based on the amino acid sequence containing the redox-active tyrosine, Y122, in the R2 subunit of Class I RNR from *E.* coli (NCBI entry, 1MXR_B[27]).

For EPR and FT-IR spectroscopic studies, the samples were dissolved in 10 mM borate-NaOH buffer, pH 11.00 ± 0.05. The sample concentration was 100 mM for FT-IR spectroscopy (unless indicated otherwise), and 16 mM for EPR spectroscopy.

NMR Spectroscopy. NMR spectra of pentapeptides were recorded at room temperature on a Bruker DRX-500 NMR spectrometer operating at 500.13 MHz using a 5 mm probe equipped with Z gradients. The water peak was suppressed using a standard Watergate sequence. The samples were suspended in 10 mM borate-NaOH buffer, pH 11, containing 10% (v/v) D_2O (purchased from Cambridge Isotope Laboratories, Andover, MA). The Shigemi (Allison Park, PA) sample tubes were susceptibility matched to D_2O.

EPR Spectroscopy. EPR spectra were recorded in polycrystalline samples at 85 K on a Bruker EMX 6/1 (Billerica, MA) X-band EPR spectrometer with ST-9605 cavity and a Dewar

insert (Wilmad Glass, Buena, NJ). The samples were placed into fused quartz sample tubes (3 mm i.d.) and frozen to 85 K under a flow of cooled nitrogen gas inside of the Dewar. A strong pitch EPR standard, $g = 2.0028 \pm 0.0002$ (Bruker) was used for the cavity calibration and for calculation of the field offset. After recording of a background EPR spectrum for each sample, the spectrometer was switched to a time sweep with magnetic field set to 3271.5 G, and trains of flashes were fired at 6.5 s intervals from a Surelite III Nd:YAG laser (Continuum, Santa Clara, CA; wavelength, 266 nm quadrupled output; flash energy, 115 mJ; pulse width, 7 ns). The energy density incident at the EPR cavity was 234 mJ cm^{-2}, and it was attenuated as necessary with a 44% transmittance beam splitter, with a concave lens, and by increasing the laser Q-switch delay. The flash energy was measured with a Scientech (Boulder, CO) Vector S310 meter with a PHD50 pyroelectric detector. Another EPR spectrum was collected after completion of the flash sequence, and the pre-illumination background was subtracted from this spectrum to present in Figure 2. A photolysis spectrum of the borate buffer was then subtracted. The spectrometer settings were as follows: microwave frequency, 9.21 GHz; power, 200 μW; modulation amplitude, 2 G; modulation frequency, 100 kHz; time constant, 81.92 ms; conversion time, 81.92 ms; number of scans, 8. Control experiments showed that there was no microwave power saturation under these conditions (data not shown). In the time-sweep mode, data acquisition parameters were the same, except that the magnetic field was set to 3271.5 G, the time constant was changed to 2.56 ms, and the conversion time was changed to 40.96 ms. Representative EPR spectra and kinetic traces are presented in the figures. The variation in EPR amplitudes from experiment to experiment was in the 10−15% range.

FT-IR Spectroscopy. FT-IR spectra were recorded at 85 K on a Nicolet Magna 550 II spectrometer with a MCT-A detector (Nicolet, Madison, WI) in a rapid scan mode. 6 μL liquid samples were placed between a pair of CaF_2 windows separated by a 6 μm spacer in a liquid nitrogen cryostat (R. G. Hansen & Associates, Santa Barbara, CA). 3062 interferograms were collected within 620 s at 4 cm^{-1} resolution and 5 cm s^{-1} mirror velocity. Three hundred seconds after the start of data collection, the sample was illuminated by a train of five laser flashes from a Surelite I or III Nd:YAG laser (Continuum, Santa Clara, CA; wavelength, 266 nm quadrupled output; flash energy, 34 mJ; pulse width, 7 ns) at a frequency of 10 Hz. The energy density incident at the IR sample was 58 mJ cm^{-2}; where indicated it was attenuated with a 44% transmittance beam splitter, with a concave lens, and by increasing the laser Q-switch delay. Lower energy and fewer flashes were sufficient to saturate the signal compared to the EPR experiments. This was due to the short (6 μm) path length of the FT-IR sample.

The set of interferograms was Fourier transformed in Omnic v.5.2 software (Nicolet, Madison, WI) using Happ-Genzel apodization, two levels of zero filling, and a Mertz phase correction. Processed data were averaged in Igor Pro v. 5.03 (Wavemetrics, Lake Oswego, OR) to produce the single beam spectra before (T_1) and after (T_2) illumination. Photolysis spectra, associated with the production of the radical (Figures 6−8) were calculated as $\Delta A = -\log(T_2/T_1)$. The photolysis spectrum (spline interpolated) of the borate buffer was interactively subtracted from the photolysis spectrum of each sample. For some differential spectra acquired at low excitation energy density, a smooth polynomial-fitted baseline was also subtracted from the data. The ground state absorption spectra (Figure 5) were calculated through ratio of the single beam spectrum (before photolysis) to an open beam background, which was recorded with no sample in the cryostat. The borate buffer absorbance spectrum was then interactively subtracted. All FT-IR data were obtained on three different samples and were averaged. The peak positions were determined with the Igor Pro "FindPeak" operation, which searches for a minimum or a maximum by analyzing the smoothed first and second derivatives of the waveforms.

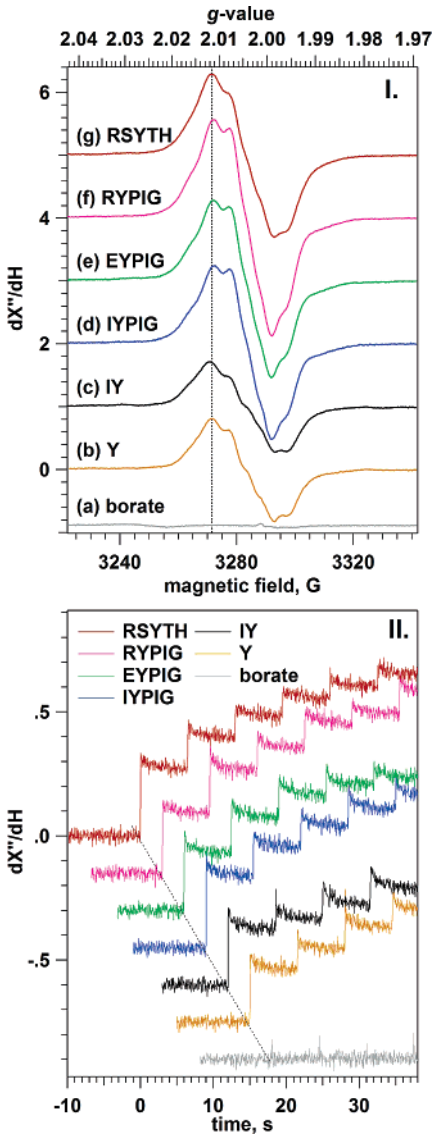

Figure 3. Panel I: 85 K EPR spectra of tyrosyl radicals generated by UV photolysis of tyrosinate Y (b), an isoleucine-tyrosine IY dipeptide (c), and the pentapeptides IYPIG, EYPIG, RYPIG and RSYTH (d−g). The spectra are displayed with vertical offsets. The sample concentration was 16 mM. The photolysis spectrum of borate buffer (a) was subtracted from all presented spectra (b−g). The vertical line indicates the peak position at 3271.5 G at which the kinetics (see panel II) were monitored. Panel II: Initial time course of the EPR amplitude at 3271.5 G upon multiple flash excitation. The traces are displayed with vertical and horizontal offsets.

Results and Discussion

EPR Spectroscopy of Tyrosyl Radical. Tyrosyl radicals were generated by UV irradiation of polycrystalline samples at 85 K and detected by EPR spectroscopy. UV photolysis of an alkaline tyrosinate solution gave rise to an EPR signal (Figure 3, panel Ib) with an apparent g-value of 2.0045 and a line shape

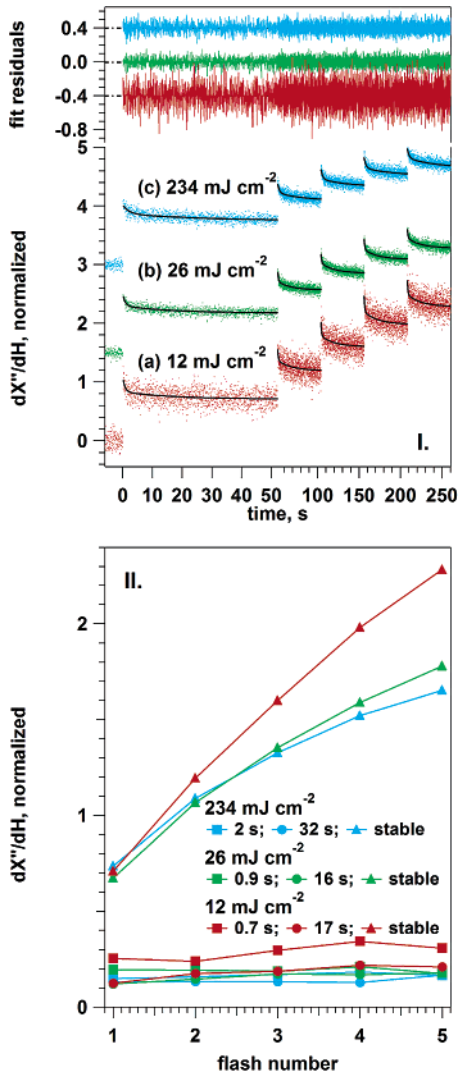

Figure 4. Panel I: Initial time course of the EPR amplitude at 3271.5 G upon multiple flash excitation of tyrosinate at three different energy densities. The sample concentration was 16 mM. The traces are displayed with vertical offsets, and the time scale of the first trace is horizontally expanded. Each signal is an average of data from three different samples and is normalized to its initial amplitude. Solid lines represent the global (two-exponential and a stable component) fits, with the residuals represented on an expanded vertical scale at the top of the panel in matching colors (see Materials and Methods for details). Panel II: The flash number dependencies of the normalized amplitudes of the two decaying components and the stable component. These kinetic components were derived from global analysis of the EPR signal kinetics in tyrosinate samples. Data were acquired at 85 K.

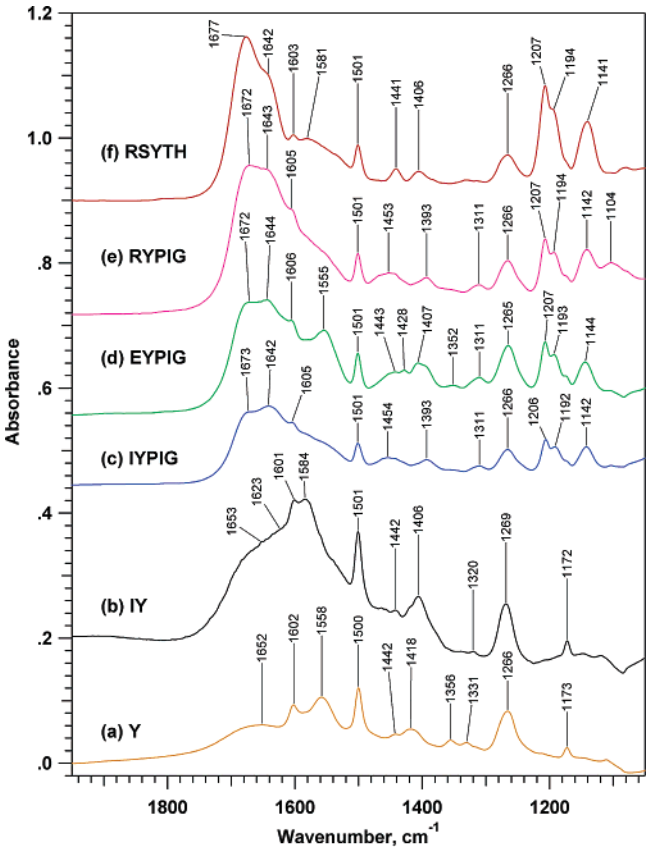

Figure 5. Ground-state FT-IR spectra of tyrosinate Y (a), the dipeptide IY (b) and the pentapeptides IYPIG (c), EYPIG (d), RYPIG (e), and RSYTH (f) at 85 K. The sample concentration was 100 mM. The data are displayed with vertical offsets.

similar to those previously reported for tyrosyl radical.[11−13] This component of the radical signal was stable between 77 and 100 K (see next section for details). The EPR line shape and the *g*-value of the radical produced in the IY dipeptide (Figure 3, panel Ic) were similar to those observed in tyrosinate (Figure 3, panel Ib) and to data previously reported.[13] Some perturbation of the EPR line shape was observed when Y and IY were compared to three pentapeptides, IYPIG (Figure 3, panel Id), EYPIG (Figure 3, panel Ie) and RYPIG (Figure 3, panel If). The EPR spectra of these three pentapeptides were similar. However, the EPR spectrum of the R2-based pentapeptide, RSYTH (Figure 3, panel Ig) was distinct from the PSII-based peptides and was more similar to the spectrum generated in tyrosinate (Figure 3, panel Ib) or in the dipeptide IY (Figure 3, panel Ic). The *g*-values of all tyrosine-containing samples were indistinguishable (range: 2.0042−2.0045), given the precision of the X-band spectrometer, which was calibrated with a strong pitch EPR standard.

We conclude that a tyrosyl radical is generated in all the pentapeptide sequences. However, the spectra reveal small differences, when the RNR and PSII-based peptides are compared. The EPR line shape results from hyperfine coupling of the unpaired electron with the 3′, 5′ ring protons and with the β-protons of the methylene group. The hyperfine interaction with the β-protons depends on the dihedral angle (θ) (Figure 1) and is thus sensitive to rotation at the C_1-C_β single bond.[10,12,28,29] Recent DFT calculations[24] on tyrosinate and tyrosyl radical have predicted that two conformers of tyrosinate are populated at room temperature, with ring dihedral angles of +168° (conformer A) and −69° (conformer B). These conformers will be frozen in at low temperatures, where large scale conformational rearrangement is prevented. On the other hand, there is only one conformer of tyrosyl radical populated at room temperature, conformer A with a ring dihedral angle of 165°. For the radical, conformer B is predicted to be 2.5 kcal/mol higher in energy when compared to conformer A.[24] Therefore, we predict that when photolysis is carried out at 85 K, the initial, populated radical states have ring dihedral angles that are representative of the tyrosinate ground state (+168 and −69°).[24] Note that the initially populated B conformational state is predicted to be unstable in the radical and should decay at higher temperatures. These predictions are in good agreement with previous experimental results.[28,29] Therefore, we hypothesize that the spectral differences observed in Figure 3, panel I, may be due to small sequence-dependent differences in the population of allowed tyrosyl radical conformers.

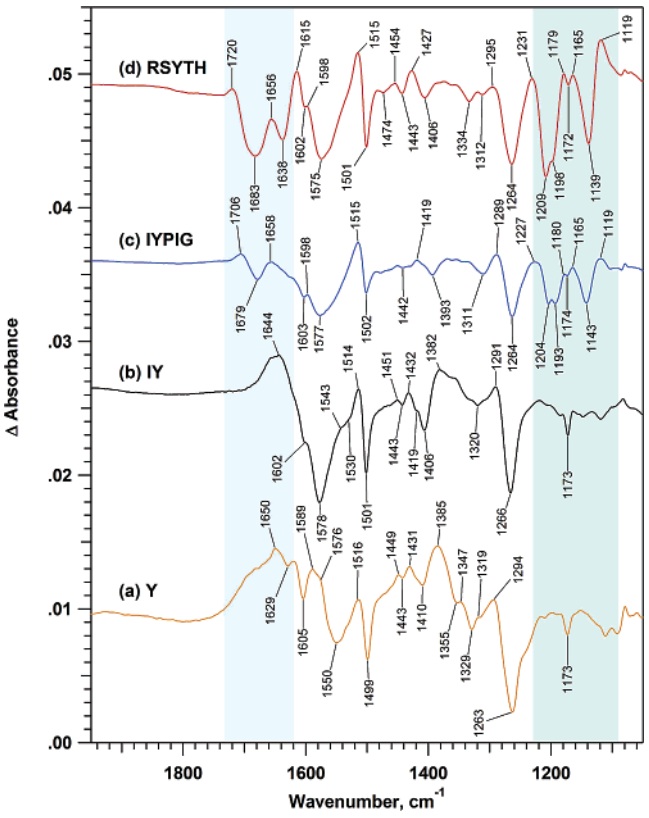

Figure 6. Photolysis-induced difference FT-IR spectra of Y (a), the dipeptide IY (b), and pentapeptides IYPIG (c) and RSYTH (d). Data were acquired at 85 K. The sample concentration was 100 mM. The photolysis spectrum of borate buffer (Figure 7f) was subtracted from each spectrum. The spectra are displayed with vertical offsets. The shaded areas represent regions assigned to the peptide backbone.

Stability of Tyrosyl Radical at Cryogenic Temperatures. Tyrosyl radical generated by UV illumination at room temperature has a lifetime of 77 μs.[30] To estimate the radical stability at 85 K, the amplitude of the EPR signal was monitored at a single field position (3271.5 G, shown in Figure 3, panel I, by the vertical line). Following a laser flash, the EPR amplitude reached a maximum within a time period shorter than conversion time (40.96 ms) of the spectrometer's digitizer, and then decayed slightly on the seconds time scale to a steady-state level. Each consecutive flash in the 50-flash sequence resulted in a smaller amplitude increment (Figure 3, panel II). The interval between the flashes in this experiment was 6.5 s (to allow acquisition of 50 traces within the 8192-point acquisition limit of the spectrometer digitizer). Neither the decay nor the stable component was observed in photolysis experiments on the borate buffer alone (Figure 3, panel Ia and IIa).

The series of 50 kinetic segments was analyzed by a global exponential fit using Igor Pro, and the best fit resolved a decaying component, with a lifetime varying from 1 to 2 s between the samples, and a stable (nondecaying) component. The stable component has the EPR line shape shown in Figure 3, panel I. The lifetime of the decaying component showed no apparent correlation with the sample type. Also, the global fit residual plots indicate that the lifetime does not vary from flash to flash (data not shown). Among the six compounds, the contribution of the minor decaying component to the overall amplitude varied from 13% to 22% for the 1st flash to 1% to 6% for the 50th flash. This corresponds to a 20−60% decrease in its absolute amplitude over the course of the multiple flash experiment. The stable component was very stable at liquid nitrogen temperature as the photoinduced EPR signal, (Figure 3, panel I) decreases only by 3−5% in its amplitude and does not change its line shape upon sample storage for 24 h at 77 K.

To obtain a better resolution of the kinetic components, tyrosinate samples were illuminated with trains of five flashes with longer (50 s) intervals between the flashes (Figure 4, panel I). Three different photon densities were employed in the 266 nm photolysis pulse. Note that the spectral line width of tyrosyl radical was independent of photolysis photon density, given the difference in signal-to-noise ratio (data not shown). Because the light-exposed sample area was larger at the lowest energy (due to use of a concave lens), the signals were first normalized to the initial amplitude (derived from a two-exponential fit), and then all five traces were analyzed by global multiexponential fitting.

Figure 4, panel I, shows the experimental data, the global fit curves, and the residuals of the fit. By analyzing the residuals and the standard deviations, we found that the best fit to these data is provided by a two-exponential function with a stable (nondecaying) component. In addition to the 1−2 s component found with the shorter interval between the flashes (Figure 3, panel II), a component with a lifetime of ca. 20 s was found in this analysis. Figure 4, panel II, shows the dependence of amplitudes on a flash number for each of the energy densities.

These data show that the fast decaying components are not caused by a photochemical or thermal artifact. Should the fast component(s) result from such an artifact, one would expect a higher contribution at higher energies. However, this is not the case, as seen from Figure 4, panel II. The contribution of the fastest, 0.7-s component was similar at all excitation energies.

We conclude that all three EPR kinetic phases arise from tyrosyl radical. Because our DFT calculations[24] and previous experimental work from other groups[28,29] point to the existence of an unstable radical conformer (see above), we interpret the relaxing phases as slight, spontaneous conformational rearrangements in a small radical population. To explain our results, these conformational rearrangements must slightly alter the EPR amplitude at the monitoring field and must be allowed at cryogenic temperatures.

Ground-State FT-IR Spectra. Figure 5 shows the ground-state spectra of tyrosinate (a), an IY dipeptide (b), and the four pentapeptides (c−f). The first two spectra are similar to previously reported spectra.[13] The most prominent difference observed in the dipeptide is the presence of a strong absorption in the amide I region (1680−1620 cm^{-1}), which overlaps with the OH bending band of water.[31] In the pentapeptides (Figure 5, parts c−f), an amide I band is also observed, as expected. The amide I band is assignable to the C═O stretching vibration of the peptide bond. This band has been used to predict secondary structural content due to its sensitivity to hydrogen bonding.[32] For pentapeptides, we expect that at room temperature there is no single, well-defined conformation, but rather that there exists an ensemble of structures, which interconvert rapidly.[33,34] When the amide I regions of the different pentapeptides are compared at cryogenic temperatures, the FT-IR absorption spectra (Figure 5, parts c−f) show only small frequency variations, which are probably caused by changes in relative amplitude in this region. For example, all the spectra show two similar components between 1677 and 1672 and 1644−1642 cm^{-1} (Figure 5, parts c−f). Because no large frequency variations are observed, these FT-IR absorption data provide no evidence for large changes in the average, trapped cryogenic conformation as a function of sequence. However, *small* changes in average conformation cannot be ruled out. In addition, these data provide no evidence for intermolecular

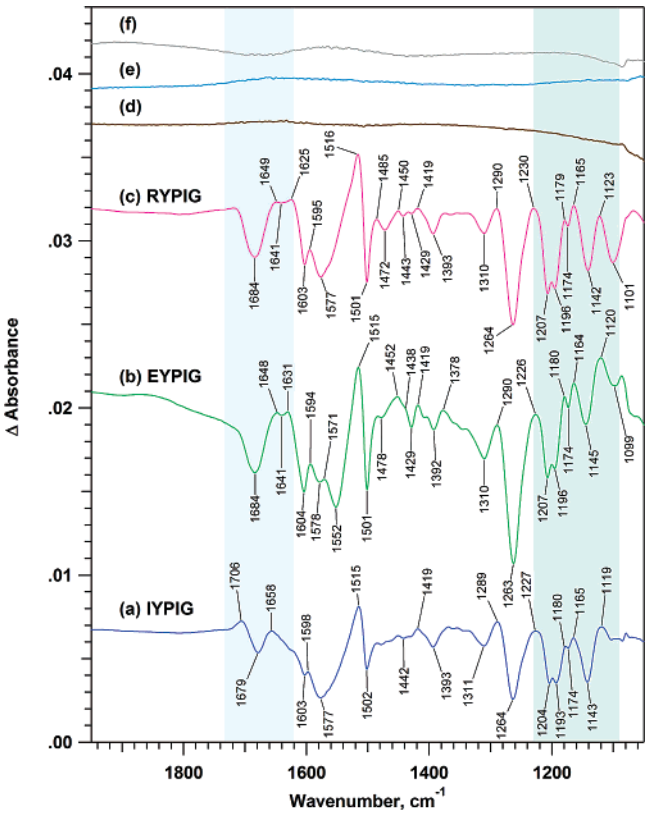

Figure 7. Photolysis-induced difference FT-IR spectra of IYPIG (a), EYPIG (b) and RYPIG (c), two control peptides, RE (d) and polyalanine (e), and borate buffer (f). The sample concentration was 100 mM, except for polyalanine, where the concentration was estimated as ~15−75 mM, based on the molecular mass range provided by the manufacturer. The photolysis spectrum of borate buffer (f) was subtracted from each pentapeptide's spectrum (a−c), but the control spectra (d−e) are presented without the buffer subtraction. Data were acquired at 85 K. The spectra are displayed with vertical offsets. The shaded areas represent regions assigned to the peptide backbone.

hydrogen bonding,[32] which would occur if higher molecular weight oligomers were formed. Note that the pentapeptide samples (Figure 5, parts c−f) also exhibit bands in the 1200−1050 cm^{-1} region, which may be assigned to skeletal stretching vibrations of the peptide bond (see discussion below).[35,36] As expected, these bands are not present in tyrosinate or in the IY dipeptide (Figure 5, parts a and b).

Differential FT-IR Spectra. Figure 6 shows the photolysis-induced difference spectra of tyrosinate (a), a dipeptide IY (b), and two pentapeptides, IYPIG (c) and RSYTH (d), which are based on the sequences of the redox-active tyrosine domains in PSII and RNR, respectively. These spectra will reflect vibrational perturbations due to oxidation of tyrosinate to produce the radical. Figure 7 compares the spectrum of IYPIG (a) with those of EYPIG (b) and RYPIG (c), which are variants of the PSII sequence in which the terminal isoleucine has been replaced by a glutamic acid or an arginine. This substitution will modulate the peptide charge. The spectra of two control peptides, RE (d) and polyalanine (e), and of the borate buffer (f) are also shown in Figure 7 (parts d−f). As expected, photolysis produces no vibrational bands in any of the borate, RE, or polyalanine samples, which do not contain tyrosine.

Assignments of the differential absorbance bands observed in the tyrosine-containing samples are based on correlations with previously published data[8,9,13,25,37−40] and our recent density-functional calculations of tyrosyl radical.[24] Unique vibrational bands of tyrosinate (Figure 6a) are observed as negative spectral features. Negative bands from tyrosinate are observed at 1605−1602 (υ_{8a/NH_2} bend), 1502−1499 (υ_{19a}), 1266−1263 ($\upsilon_{7a'}$) and 1174−1172 (υ_{9a}) cm^{-1}. To summarize, two symmetric ring stretching (υ_{8a}, υ_{19a}) bands and the CO stretching ($\upsilon_{7a'}$) and CH bending (υ_{9a}) vibrational modes are observed in the photolysis spectra of tyrosinate (Figure 6a).[13,30] These bands are also observed in the dipeptide (Figure 6b) and all the pentapeptide samples (Figure 6, parts c and d; Figure 7, parts a−c) at similar frequencies. In the dipeptide and pentapeptides, oxidation also perturbs the frequency of a negative band at 1578−1575 cm^{-1} (Figure 6, parts b−d). This band may be assigned to a combination of the ring υ_{8b} stretching vibration, a carboxylate stretching mode, and an NH_2 bending mode.[24] The corresponding band is observed at 1550 cm^{-1} in the tyrosinate samples (Figure 6, a).[13,24]

Oxidation of tyrosine is known to perturb the frequency of the CO stretching and ring stretching vibrations.[8,9,13] Unique vibrational modes of the radical will be positive bands in the photolysis spectra. A tyrosyl radical NH_2 bending/CO_2 stretching band[13,24] contributes to the spectrum at ~1640 cm^{-1}; this band overlaps a positive contribution from the OH_2 bending mode of the solvent. The broad υ_{8a} stretching vibration of the radical is observed at ~1560−1550 cm^{-1}, where it also overlaps other spectral contributions. A positive band at 1516−1514 cm^{-1} is observed in all samples and corresponds to υ_{7a} (the CO stretching) vibration of the radical.[13,24] Observation of tyrosinate and tyrosyl radical bands in the photolysis-derived FT-IR spectrum confirms that a tyrosyl radical is generated in each sample, as expected from the EPR results presented in Figure 3, panel I. The relative amplitudes of the ~1515 and ~1265 cm^{-1} bands give a measure of radical yield under the FT-IR conditions.

In our previous work, ^{15}N sensitive bands in the photolysis spectrum of tyrosinate at 1647/1627/1603 cm^{-1} were assigned to NH_2 bending modes. The observation of these bands was attributed to a delocalization of spin to the amino group.[13] In the photolysis spectrum of dipeptides, candidates for amide I (C═O stretch)[35] and amide II (combination CN stretch, NH bend)[35] bands were observed. For example, in the dipeptide HY, derivative-shaped bands at 1628 (−)/1620 (+) and 1548 (+)/1531 (−) cm^{-1} were assigned to amide I (C═O stretching) and amide II (C−N stretching, NH bending) modes, respectively.[13] In the dipeptide IY, a 1543 (+)/1531 (−) cm^{-1} shoulder was assigned to an amide II band and an inflection point at 1622 cm^{-1} was suggested to arise from an amide I band (see ref 13 and also Figure 6b). Observation of amide I and II bands in dipeptides was attributed to spin delocalization to the amide bond.[13] In dipeptides, there is no transition dipole coupling to complicate spectral interpretation, and the amide I band is observed at low frequency relative to the amide I band in polypeptides and proteins.

As shown in Figures 6 and 7, all the pentapeptide spectra exhibit a ~1543 cm^{-1} shoulder on the CO stretching band, which may be assignable to an amide II vibration. In addition, all pentapeptides (Figures 6 and 7) display derivative-shaped bands in the 1680−1620 cm^{-1} polypeptide amide I region.[35] These derivative-shaped bands have a negative component between 1684 and 1679 cm^{-1} and a positive component between 1658 and 1648 cm^{-1}. This observation is consistent with a perturbation of the amide I force constant by oxidation of the aromatic ring. Interestingly, in RSYTH, an additional 1638 (−)/1615 (+) cm^{-1} band (Figure 6d) is also observed in the amide I region. This is an indicator of sequence-specific interactions between the tyrosyl radical and the amide bond.

All pentapeptides also exhibit derivative-shaped bands in the photolysis spectra in the 1230−1090 cm^{-1} region (Figure 6, parts c and d; Figure 7, parts a−c), which are not present in the tyrosinate and in the dipeptide. These bands of the photolysis spectra result from perturbation of three spectral bands in the ground-state spectra at 1207−1206, 1194−1192, and 1144−1141 cm^{-1} (Figure 5, parts c−f). In the pentapeptides, these bands overlap the 1173−1172 cm^{-1} band (CH bending υ_{9a}), which are also present in spectra of tyrosinate and the dipeptide IY. In the photolysis spectrum of IYPIG (Figure 6c), the 1204 /1193 cm^{-1} pair shifts down to 1180/1165 cm^{-1} and the 1143 band shifts to 1119 cm^{-1}. In the photolysis spectrum of RSYTH (Figure 6d), the 1209 /1198 cm^{-1} pair shifts to 1179/1165 cm^{-1} and the 1139 band shifts to 1119 cm^{-1}.

Assignments in this spectral region are complex. In previous Raman and infrared studies, spectral bands in the 1200−1050 cm^{-1} were assigned to CH_3 rocking vibrations, along with C−C and C−N backbone skeletal stretches.[35,41] Other spectral contributions are also possible. The higher frequency bands are similar in frequency to the calculated frequencies for the NC^{α} and the $C^{\alpha}C^{\beta}$ stretch in polyalanine, while the third band is close in its frequency to NC^{α} and $C^{\alpha}C^{\beta}$ stretching vibrations observed in polyglycine.[35] A 1204 cm^{-1} band in collagen was attributed either to amide III or CH_2 wagging vibration.[42] Note that the ground state spectrum of polyalanine has weak and relatively broad bands at 1213 and 1190 cm^{-1} (not shown), which were not perturbed, as expected, in photolysis spectrum (Figure 7e).

Taken together, these reports suggest that these 1230−1090 cm^{-1} bands are associated with the vibrations of the peptide backbone. To explain their appearance in the photolysis spectrum, we propose that oxidation of the aromatic ring alters the force constants of these normal modes, as well as the force constants of the amide I and II bands. The frequencies of some of these bands do not exhibit marked sequence dependency. In EYPIG (Figure 7b), the bands are observed at 1207/1196 cm^{-1}, 1180/1164 cm^{-1} and 1145/1120 cm^{-1}, while in RYPIG (Figure 7c) the bands are observed at 1207/1196, 1179/1165, and 1142/1123 cm^{-1}. However, we note the presence of a sequence-specific band at 1101 cm^{-1} in RYPIG (Figure 7c) and less prominent 1099 cm^{-1} band in EYPIG (Figure 7b); these bands are not noticeable in the other pentapeptides. Similar frequencies (1105 and 1108 cm^{-1}) were reported in Raman and infrared spectra of polyalanine.[35]

The spectra in Figure 7b also provide evidence for perturbation of an amino acid side chain, adjacent to the redox-active tyrosine. In the spectrum of EYPIG, a variant of the D1 sequence, in which the amino terminal isoleucine has been replaced by a glutamic acid to add extra negative charge, differential features at 1571 (+)/1552 (−) and 1438 (+)/1429 (−) are observed (Figure 7b). These unique bands are not present either in the IYPIG pentapeptide based on the original D1 sequence or in the RYPIG peptide in which isoleucine has been replaced by arginine to add extra positive charge. These frequencies are consistent with oxidation-induced perturbation of the asymmetric and symmetric stretching vibration of the adjacent carboxylic acid side chain.[43]

Photolysis Spectra Observed at Lower Photon Densities and at Lower Sample Concentrations. To rule out the possibility that bands in the photolysis spectra are due to multiphoton processes, secondary products, and sample decomposition, we report FT-IR photolysis spectra of tyrosinate and two pentapeptides at excitation energy densities 7.25 times lower than used in the FT-IR experiments described above. As seen from Figure 8, panel I, the spectra collected at the two different energy densities consist of the same set of differential bands, although the signal-to-noise ratio is lower in the case of low excitation energy. At lower signal-to-noise, a background contribution from the ground-state absorption spectrum becomes more obvious. This background contribution resembles a roll in the differential spectrum baseline. Importantly, the sets of spectral features in the amide I region and in 1230−1090 cm^{-1} region are well resolved in both IYPIG (Figure 8b) and RSYTH (Figure 8c) at significantly lower energy densities.

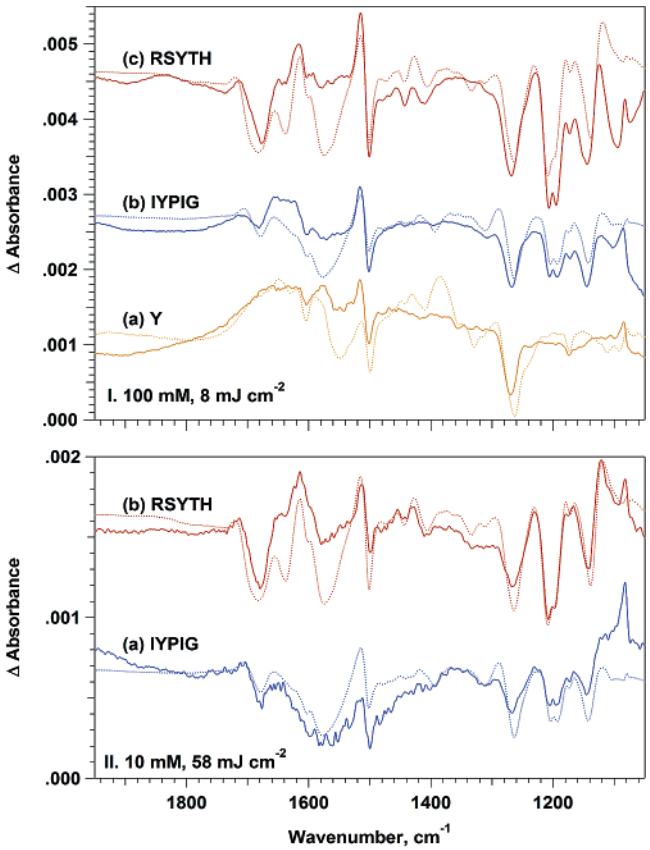

Figure 8. Panel I: Photolysis-induced difference FT-IR spectra of tyrosinate Y (a, solid line), IYPIG (b, solid line) and RSYTH (c, solid line) with lower photon density (8 mJ cm^{-2}) in the photolysis pulse. The dotted lines show the spectra of the corresponding pentapeptides, acquired with the standard excitation energy (58 mJ cm^{-2}). Panel II: Photolysis-induced difference FT-IR spectra of IYPIG (a, solid line) and RSYTH (b, solid line) at a concentration of 10 mM. Dotted lines represent the spectra of the corresponding pentapeptides at 100 mM on an arbitrary scale for presentation purposes. See Figure 6 for correct scale. Data were acquired at 85 K. The spectra are displayed with vertical offsets.

To verify whether any of the observed differential spectral features could be related to aggregation of the pentapeptides at a concentration of 100 mM, differential FT-IR spectra of two pentapeptides, IYPIG and RSYTH, were also acquired at 10 mM (Figure 8, panel II). The observed similarity of the 10 and 100 mM photolysis spectra (except for the difference in signal-to-noise) indicates that the differential bands do not arise from artifacts due to molecular aggregation. Another independent verification that aggregation does not occur in these peptides under these conditions (borate buffer, pH 11) is the one-dimensional NMR spectrum, which is sensitive to oligomeric state.[44] Figure 9 shows ^1H NMR spectra of two pentapeptides, IYPIG (a, b) and RSYTH (c, d) at 10 and 100 mM concentrations. The common features of these spectra include peaks in the 6.5−7.0 ppm range, which can be ascribed to aromatic ring

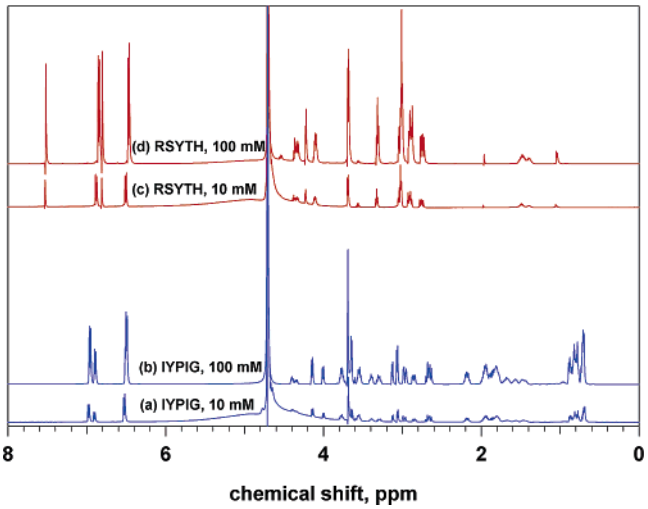

Figure 9. Room temperature ^{1}H NMR spectra of 10 mM IYPIG (a), 100 mM IYPIG (b), 10 mM RSYTH (c), and 100 mM RSYTH (d). The spectra are displayed with vertical offsets.

protons, and sets of peaks at 4.2 ppm (α-proton) and at 2.7 ppm (β-protons).[45] The unique peak at ~7.5 ppm in RSYTH can be ascribed to ring protons of histidine residue, and unique features in the 0.7−0.9 ppm range in IYPIG can be ascribed to the β-protons in isoleucine.[45] Most importantly, the observed ^{1}H NMR peak line widths for the two pentapeptides, IYPIG and RSYTH are indistinguishable at 10 and 100 mM concentrations, and therefore there is no evidence of the line broadening associated with peptide oligomerization. These NMR results support conclusions reached from our analysis of the ground-state FT-IR spectrum (see discussion earlier).

Conclusions. In this paper, we report several novel findings concerning the photophysical properties of tyrosyl radicals in peptides. First, we find that the EPR line shape of the radical depends on peptide sequence. Second, we present evidence for a decaying component of the EPR signal of tyrosyl radical. We assign this transient to a spontaneous, small structural rearrangement in the radical. Third, we show that amide I vibrational modes and peptide bond skeletal stretch bands are observed in the photolysis spectra of tyrosine-containing pentapeptides. From these data, we conclude that oxidation of the tyrosine aromatic ring perturbs the electronic structure of the peptide bond in tyrosine-containing oligopeptides. Fourth, we report sequence-dependent alterations in these bands, suggesting that the perturbative mechanism depends either on conformation or electrostatics.

We interpret the perturbative mechanism to be spin density delocalization to the amide group, in agreement with previous DFT calculations.[13,20,21] Other possible mechanisms for this perturbation can be considered. One possibility is that an intermolecular interaction between the pentapeptides perturbs the amide bond. However, such an interpretation is not supported by the finding that the photolysis spectra, acquired at 10 and 100 mM, are similar. It is also not supported by the NMR spectra, reported here and recorded at these two concentrations. A second possibility is that there is an intramolecular change in hydrogen bonding, which is induced by photolysis, and that this hydrogen bonding involves the peptide bond. However, a direct interaction between the tyrosyl radical and the peptide nitrogen is very unlikely, due to steric constraints. A third possibility is that conformational rearrangement or changes in solvation may underlie the observed perturbation. These possibilities cannot be excluded, but because the experiments were conducted at cryogenic temperatures, these changes must be subtle, if they occur. Note that a solvation shell perturbation upon tyrosinate oxidation has been previously reported. [13]

Our work suggests that primary structure has an impact on the structure and function of redox-active tyrosine residues. Secondary and tertiary structural interactions are also expected to influence reactivity; in future work, the impact of these additional control mechanisms on tyrosyl radicals will be explored.

Acknowledgment. This work was supported by NIH Grant GM43273. The authors thank Dr. Leslie Gelbaum and Ms. Robin Sibert for their help in collection and processing of NMR data.

References and Notes

(1) Tsai, A.; Kulmacz, R. J.; Palmer, G. *J. Biol. Chem.* **1995**, *270*, 10503.
(2) Whittaker, M. M.; DeVito, V. L.; Asher, S. A.; Whittaker, J. W. *J. Biol. Chem.* **1989**, *264*, 7104.
(3) Sjöberg, B. M.; Reichard, P.; Gräslund, A.; Ehrenberg, A. *J. Biol. Chem.* **1978**, *253*, 6863.
(4) Barry, B. A.; Babcock, G. T. *Proc. Natl. Acad. Sci. U.S.A.* **1987**, *84*, 7099.
(5) Boerner, R. J.; Barry, B. A. *J. Biol. Chem.* **1993**, *268*, 17151.
(6) Land, E. J.; Porter, G.; Strachan, E. *Trans. Faraday Soc.* **1961**, *57*, 1885.
(7) Dixon, W. T.; Moghimi, M.; Murphy, D. *J. Chem. Soc., Faraday Trans. 2* **1974**, *70*, 1713.
(8) Tripathi, G. N. R.; Schuler, R. H. *J. Chem. Phys.* **1984**, *81*, 113.
(9) Johnson, C. R.; Ludwig, M.; Asher, S. A. *J. Am. Chem. Soc.* **1986**, *108*, 905.
(10) Svistunenko, D. A.; Cooper, C. E. *Biophys. J.* **2004**, *87*, 582.
(11) Hulsebosch, R. J.; van der Brink, J. S.; Nieuwenhuis, S. A. M.; Gast, P.; Raap, J.; Lugtenburg, J.; Hoff, A. J. *J. Am. Chem. Soc.* **1997**, *119*, 8685.
(12) Barry, B. A.; El-Deeb, M. K.; Sandusky, P. O.; Babcock, G. T. *J. Biol. Chem.* **1990**, *265*, 20139.
(13) Ayala, I.; Range, K.; York, D.; Barry, B. A. *J. Am. Chem. Soc.* **2002**, *124*, 5496.
(14) Babcock, G. T.; Espe, M.; Hoganson, C.; Lydakis-Simantiris, N.; McCracken, J.; Shi, W. J.; Styring, S.; Tommos, C.; Warncke, K. *Acta Chem. Scand.* **1997**, *51*, 533.
(15) Gräslund, A.; Sahlin, M. *Annu. Rev. Biophys. Biomol. Struct.* **1996**, *25*, 259.
(16) Warncke, K.; Babcock, G. T.; McCracken, J. *J. Am. Chem. Soc.* **1994**, *116*, 7332.
(17) Hoganson, C. W.; Sahlin, M.; Sjöberg, B. M.; Babcock, G. T. *J. Am. Chem. Soc.* **1996**, *118*, 4672.
(18) Tommos, C.; Tang, X. S.; Warncke, K.; Hoganson, C. W.; Styring, S.; McCracken, J.; Diner, B. A.; Babcock, G. T. *J. Am. Chem. Soc.* **1995**, *117*, 10325.
(19) Hoganson, C. W.; Babcock, G. T. *Biochemistry* **1992**, *31*, 11874.
(20) Barry, B. A.; Einarsdóttir, Ó. *J. Phys. Chem. B* **2005**, *109*, 6972.
(21) Pujols-Ayala, I.; Barry, B. A. *Biochim. Biophys. Acta* **2004**, *165*, 205.
(22) Tripathi, G. N. R.; Schuler, R. H. *J. Chem. Soc., Faraday Trans.* **1993**, *89*, 4177.
(23) Campbell, K. A.; Peloquin, J. M.; Diner, B. A.; Tang, X. S.; Chisholm, D. A.; Britt, R. D. *J. Am. Chem.* Soc. **1997**, *119*, 4787.
(24) Range, K.; Ayala, I.; York, D.; Barry, B. A. Submitted.
(25) Pujols-Ayala, I.; Sacksteder, C. A.; Barry, B. A. *J. Am. Chem. Soc.* **2003**, *125*, 7536.
(26) Kamiya, N.; Shen, J. R. *Proc. Natl. Acad. Sci. U.S.A.* **2003**, *100*, 98.
(27) Högbom, M.; Galander, M.; Andersson, M.; Kolberg, M.; Hofbauer, W.; Lassmann, G.; Nordlund, P.; Lendzian, F. *Proc. Natl. Acad. Sci. U.S.A.* **2003**, *100*, 3209.
(28) Warncke, K.; Babcock, G. T.; McCracken, J. *J. Phys. Chem.* **1996**, *100*, 4654.
(29) Warncke, K.; Perry, M. S. *Biochim. Biophys. Acta* **2001**, *1545*, 1.
(30) Cappuccio, J. A.; Ayala, I.; Elliot, G. I.; Szundi, I.; Lewis, J.; Konopelski, J. P.; Barry, B. A.; Einarsdóttir, Ó. *J. Am. Chem. Soc.* **2002**, *124*, 1750.
(31) Bellamy, L. J. *The infrared spectra of complex molecules*; Chapman and Hall: London, 1980; Vol. II.
(32) Torii, H.; Tasumi, M. Theoretical analyses of the amide I infrared bands of globular proteins. In *Infrared spectroscopy of biomolecules*; Mantsch, H. H., Chapman, D., Eds.; Wiley-Liss: New York, 1996; p 1.

(33) Meirovitch, E.; Meirovitch, H. *Biopolymers* **1996**, *38*, 69.
(34) Bogusky, M. J.; Naylor, A. M.; Pitzenberger, S. M.; Nutt, R. F.; Brady, S. F.; Colton, C. D.; Sisko, J. T.; Anderson, P. S.; Veber, D. *Int. J. Pept. Protein Res.* **1992**, *39*, 63.
(35) Krimm, S.; Bandekar, J. *Adv. Protein Chem.* **1986**, *38*, 181.
(36) Nauman, D. FT-infrared and FT-Raman spectroscopy in biomedical research. In *Infrared and Raman spectroscopy of Biological materials*; Gremlich, H.-U., Yan, B., Eds.; Marcel Dekker: New York, 2001; p 323.
(37) Nwobi, O.; Higgins, J.; Zhou, X.; Liu, R. *Chem. Phys. Lett.* **1997**, *272*, 155.
(38) Takeuchi, H.; Watanabe, N.; Satoh, Y.; Harada, I. *J. Raman Spectrosc.* **1989**, *20*, 233.
(39) Mukherjee, A.; McGlashen, M. L.; Spiro, T. G. *J. Phys. Chem.* **1995**, *99*, 4912.
(40) Chipman, D. M.; Liu, R.; Zhou, X.; Pulay, P. *J. Chem. Phys.* **1994**, *100*, 5023.
(41) Ford, S. J.; Wen, Z. Q.; Hecht, L.; Barron, L. D. *Biopolymers* **1994**, *34*, 303.
(42) Jackson, M.; Mantsch, H. H. Biomedical infrared spectroscopy. In *Infrared spectroscopy of biomolecules*; Mantsch, H. H., Chapman, D., Eds.; Wiley-Liss: New York, 1996; p 311.
(43) Hutchison, R. S.; Steenhuis, J. J.; Yocum, C. F.; Razeghifard, M. R.; Barry, B. A. *J. Biol. Chem.* **1999**, *274*, 31987.
(44) Cavanagh, J.; Fairbrother, W. J.; Palmer, A. G.; III; Skelton, N. J. *Protein NMR spectroscopy: Principles and practice*; Academic Press: San Diego, CA, 1996.
(45) Wüthrich, K. *NMR of proteins and nucleic acids*; John Wiley & Sons: 1986.